JGR Atmospheres

RESEARCH ARTICLE
10.1029/2018JD029553

This article is a companion to Zambri et al. (2019), https://doi.org/10.1029/2018JD029554.

Key Points:
- Simulations indicate that the Laki aerosol cloud was transported globally, with peak aerosol effective radii of 0.4 micrometers at Northern Hemisphere high latitudes
- The simulated Laki aerosol cloud affects circulation globally, strengthening the Southern Annular Mode and weakening the Northern Annular Mode
- Induced temperature gradients and wave driving both contribute to the polar vortex response

Supporting Information:
- Supporting Information S1

Correspondence to:
B. Zambri,
bzambri@mit.edu

Citation:
Zambri, B., Robock, A., Mills, M. J., & Schmidt, A. (2019). Modeling the 1783–1784 Laki eruption in Iceland: 1. Aerosol evolution and global stratospheric circulation impacts. *Journal of Geophysical Research: Atmospheres*, *124*, 6750–6769. https://doi.org/10.1029/2018JD029553

Received 27 AUG 2018
Accepted 2 MAY 2019
Accepted article online 13 MAY 2019
Published online 4 JUL 2019

Modeling the 1783–1784 Laki Eruption in Iceland: 1. Aerosol Evolution and Global Stratospheric Circulation Impacts

Brian Zambri[1,2], Alan Robock[1], Michael J. Mills[3], and Anja Schmidt[4,5]

[1]Department of Environmental Sciences, Rutgers University, New Brunswick, NJ, USA, [2]Now at Department of Earth, Atmospheric, and Planetary Sciences, Massachusetts Institute of Technology, Cambridge, MA, USA, [3]Atmospheric Chemistry Observations and Modeling Laboratory, National Center for Atmospheric Research, Boulder, CO, USA, [4]Department of Chemistry, University of Cambridge, Cambridge, UK, [5]Department of Geography, University of Cambridge, Cambridge, UK

Abstract The 1783–1784 CE Laki flood lava eruption began on 8 June 1783. Over the course of 8 months, the eruption released approximately 122 Tg of sulfur dioxide gas into the upper troposphere and lower stratosphere above Iceland. Previous studies that have examined the impact of the Laki eruption on sulfate aerosol and climate have either used an aerosol model coupled off-line to a general circulation model (GCM) or used a GCM with incomplete aerosol microphysics. Here, we study the impact on stratospheric aerosol evolution and stratospheric and tropospheric circulation using a fully coupled GCM with complete aerosol microphysics, the Community Earth System Model version 1, with the Whole Atmosphere Chemistry Climate Model high-top atmosphere component. Simulations indicate that the Laki aerosols had peak average effective radii of approximately 0.4 μm in Northern Hemisphere (NH) middle and high latitudes, with peak average effective radii of 0.25 μm in NH tropics and 0.2 μm in the Southern Hemisphere. We find that the Laki aerosols are transported globally and have significant impacts on the circulation in both hemispheres, strengthening the Southern Hemisphere polar vortex and shifting the tropospheric NH subtropical jet equatorward.

1. Introduction

The 1783–1784 CE Laki eruption began on 8 June 1783 and was one of the largest flood lava eruptions in recent history, emitting ~122 Tg of sulfur dioxide (SO_2) into the upper troposphere/lower stratosphere above Iceland during its 8-month duration (Thordarson et al., 1996). The eruption had far-reaching consequences, including widespread atmospheric pollution and environmental devastation (Thordarson, 1995; Thordarson et al., 1996; Thordarson & Self, 2003). Thordarson and Self (2003), the most detailed review of the Laki eruption and its aftermath, included a detailed budget of the emissions released from Laki. Several numerical modeling studies of the Laki impacts have used those emissions (Stevenson et al., 2003; Highwood & Stevenson, 2003; Oman, Robock, Stenchikov, & Thordarson, 2006, Oman, Robock, Stenchikov, Thordarson, Koch, et al., 2006; Schmidt et al., 2010, 2012; Pausata, Chafik, et al., 2015, Pausata, Grini, et al., 2015; Pausata et al., 2016). Stevenson et al. (2003) studied the impact of the eruption on atmospheric composition using a chemical transport model, estimating that the eruption produced a total of 71–92 Tg of sulfate aerosol based on the Laki SO_2 emissions data set from Thordarson and Self (2003). In a complementary study, Highwood and Stevenson (2003) used the Reading Intermediate general circulation model (GCM) to investigate the climate impacts of the aerosol loading calculated by Stevenson et al. (2003); they found a maximum Northern Hemisphere (NH) average top-of-atmosphere net radiative perturbation of about −5.5 W/m^2 in August 1783 and an annual mean NH temperature anomaly of −0.21 K. Oman, Robock, Stenchikov, Thordarson, Koch et al. (2006) used the Goddard Institute for Space Studies ModelE GCM coupled to a sulfur chemistry scheme (Koch et al., 2006) to simulate the Laki aerosol cloud. They estimated that the Laki eruption yielded between 163 and 166 Tg of total volcanic sulfate aerosol. Schmidt et al. (2010) used a global aerosol model and found a total volcanic sulfate aerosol yield of 155 Tg. More recently, Pausata, Grini, et al. (2015) used the Norwegian Earth System Model, which included online calculation of aerosols, to simulate the Laki eruption. Unlike the previous Laki studies, Pausata, Grini, et al. (2015) only loosely followed the emissions reported by Thordarson and Self (2003), instead injecting 100 Tg of SO_2 over eight eruptive episodes, each spaced 15 days apart and each lasting 4 days. Due to incomplete aerosol microphysics, their simulations yielded a small effective radius of about 0.2 μm for the sulfate aerosol, which resulted in a very large radiative forcing, with a NH average top of atmosphere net forcing below −20 W/m^2, and a NH average temperature anomaly below −2.5 K in the months following the onset of the eruption.

In addition to the uncertainties of the physical properties of the Laki aerosols due to the use of GCMs with varied treatments of aerosol processes as well as the use of different emissions scenarios, there are general questions regarding the extent of potential dynamical responses to this and other high-latitude volcanic eruptions. Using the Goddard Institute for Space Studies ModelE, Oman et al. (2005) found anomalies resembling a negative phase of the North Atlantic Oscillation (NAO; Hurrell, 1995) in simulations of the 1912 Katmai eruption in Alaska, due in theory to stratospheric heating by volcanic aerosols and a subsequent weakening of the stratospheric polar vortex. The NAO is an index of the wintertime variability of north-south NH sea level pressure gradients between 110°W and 70°E and north of 20°N (Hurrell, 1995), and a positive phase of the NAO has been associated with an anomalously strong polar vortex (Thompson & Wallace, 1998) or a positive phase of the Northern Annular Mode (NAM). While observations and—to varying degrees—models have shown a tendency toward a strengthened polar vortex (Barnes et al., 2016; Bittner, Schmidt, et al., 2016; Bittner, Timmreck, et al., 2016; Zambri et al., 2017; Zambri & Robock, 2016) and a positive NAO (Christiansen, 2008) in the first winter after large tropical volcanic eruptions, the circulation response to high-latitude eruptions is less well understood.

The mechanisms that force a positive NAM/NAO in the winter after a low-latitude eruption have been studied extensively (e.g.,Bittner, Schmidt, et al., 2016 ; Bittner, Timmreck, et al., 2016 ; Stenchikov et al., 2002, 2004, 2006 ; Toohey et al., 2014, 2016). They are as follows: for tropical volcanic eruptions, absorption of infrared radiation by sulfate aerosols leads to an anomalously warm equatorial lower stratosphere, increasing the equator-to-pole temperature gradient. By the thermal wind relation, the anomalous temperature gradient results in stronger westerly winds in the stratosphere. However, the heating near the equator may not be the key driver for the strengthened polar vortex at 60°N (Bittner, Timmreck, et al., 2016; Stenchikov et al., 2002; Toohey et al., 2014). Other mechanisms include a decrease in upward planetary wave flux (Stenchikov et al., 2002), though Toohey et al. (2014) found an increase in upward wave flux and southward deflection of planetary waves (Bittner, Timmreck, et al., 2016). Research has also been carried out regarding the Southern Hemisphere (SH) circulation response to low-latitude volcanic eruptions, also with mixed results (Karpechko et al., 2010; Robock et al., 2007). Specifically, Robock et al. (2007) found no SH polar vortex response to a large volcanic eruption in austral winter (June–August [JJA]). Karpechko et al. (2010) subsequently studied the SH circulation response to the El Chichón and Pinatubo eruptions. They found that Robock et al. (2007) was right that there is no response in JJA but that this was the wrong season to look for a response in the SH: Because of the stability of the SH polar vortex, planetary wave propagation plays a minimal role in the winter. Instead, Karpechko et al. (2010) found in model simulations a significant strengthening of the SH vortex in fall and spring, when planetary wave activity plays a larger role in the circulation there.

The mechanisms that would force a negative NAM/NAO after a high-latitude eruption like Laki are, in principle, the opposite of those described above for low-latitude eruptions. However, it is unclear whether this is a robust response, and whether there is enough radiation near the pole in the NH wintertime to heat the stratospheric aerosol and overcome the high level of natural variability and elicit such a dynamical response.

In this paper, we examine the evolution of the aerosol cloud and circulation response following the 1783–1784 eruption of Laki in Iceland, using an ensemble of simulations carried out with the National Center for Atmospheric Research's Community Earth System Model, version 1 (CESM1; Hurrell et al., 2013), with its high-top atmospheric component, the Whole Atmosphere Community Climate Model (WACCM; Marsh et al., 2013). Similarly to, for example, Barnes et al. (2016), we analyze the monthly evolution of the circulation so as to be able to identify robust signals that might be lost by averaging over seasons. The rest of the paper is structured as follows: In section 2 we describe the CESM1(WACCM) model and experimental setup of the Laki simulations; in section 3 we present the results, including analysis of the evolution of the Laki aerosol cloud, atmospheric temperature and circulation anomalies, annular mode responses to the Laki eruption, and the anomalous wave forcing; section 4 contains a summary and discussion of the results. In a complementary study (Zambri et al., 2019), we calculate radiative forcings and assess the surface climatic impact of the Laki eruption.

2. Model Description and Experiment Setup

CESM1 is composed of interactive atmosphere, ocean, land, and sea ice components. For these experiments, we used WACCM, the high-top atmospheric component of CESM1. WACCM has 70 vertical levels, a model top of 5.1×10^{-6} hPa and 0.9° latitude × 1.25° longitude horizontal resolution, with interactive atmospheric chemistry, radiation, and dynamics. In these simulations we use the version of WACCM described by Mills et al. (2017). This version of the model includes more realistic formulations of radiation, cloud microphysics, and aerosols than past versions. Direct effects of aerosols are included in the radiation code, and indirect effects of sulfur, including sulfate aerosols, are included in the cloud microphysics (Gettelman et al., 2010; Morrison & Gettelman, 2008).

A three-mode prognostic modal aerosol model (MAM3; Liu et al., 2012) is used to represent aerosols in WACCM. MAM3 represents the aerosols in Aitken, accumulation, and coarse modes and has been modified to simulate the evolution of stratospheric sulfate aerosols from volcanic and nonvolcanic emissions (Mills et al., 2016). MAM3 is capable of representing aerosol microphysical processes, such as nucleation, condensation, coagulation, and sedimentation, and calculates new particle formation using a parameterization of sulfuric acid-water homogeneous nucleation (Vehkamäki et al., 2002). The model has been shown to perform well for both large- and small-magnitude eruptions, as well as for nonvolcanic aerosols (Mills et al., 2016, 2017; Schmidt et al., 2018).

The 1783–1784 Laki eruption began on 8 June 1783 and lasted for 8 months. According to Thordarson and Self (2003), the eruption injected a total of 122 Tg of SO_2 into the atmosphere, about 94 Tg of which was injected into the upper troposphere/lower stratosphere between 9 and 13 km. Another 28 Tg of SO_2 was emitted at the surface from lava degassing. These estimates were originally derived by Thordarson et al. (1996), using the petrologic method. Briefly, they estimated the amount of SO_2 released based on the sulfur concentrations found in Laki eruption products (e.g., tephra) from 12 different locations along the lava flow and eruption fissures, comparing the composition of undegassed lava samples to those of degassed samples. Thordarson et al. (1996) report uncertainties up to ±17% in the sulfur concentrations; Stevenson et al. (2003) suggested uncertainties could be upward of ±20% when including uncertainties in the total volume of magma released. We simulated the eruption by injecting 94 Tg of SO_2 over 10 eruptions from 8 June to 25 October; the individual explosive eruption episodes range from injections of 2.9 to 18.7 Tg of SO_2 (Figure 1). For each explosive episode, our simulated emissions occur over a 6-hr period from 1200 to 1800 UTC. The SO_2 gas from the explosive episodes is injected in a layer from 9 to 13 km. At the same time, we simulated SO_2 emitted by lava degassing by injecting an additional 28 Tg of SO_2 into the lowest model level from 8 June 1783 to 7 February 1784, continuously over the 8-month period.

We initialized the model simulations based on the synoptic conditions reported over Europe around 8 June 1783, the first day of the Laki eruption (Kington, 1988; Thordarson & Self, 2003). We chose four sets of initial conditions from a 25-year control run that best matched those observations, but the background state of the global circulation varied among the four initial conditions. For each set of initial conditions, we generated 10 ensemble members by perturbing the initial temperature field. By averaging over different background states, we can extract the volcanically forced signal. We ran one 40-member ensemble (four different initial years, 10 perturbed ensemble members for each year) with the Laki eruption (Laki) and one 40-member ensemble without the eruption (noLaki). All ensemble members are initialized on 8 June, the first day of the Laki eruption, and each simulation was 12 months long.

We use two methods to calculate anomalies: In the first, we subtract the mean of the 5 years before the eruption; in the other, we subtract the noLaki ensemble mean. Pausata, Grini, et al. (2015) found differences in the perceived forced surface climate response to a Laki-like volcanic eruption, based on both the method of initialization and the method of calculating anomalies; here we similarly analyze the impacts of the choice of anomaly period on the forced response in the circulation. We analyzed daily and monthly means of model outputs, and we assess statistical significance using two methods: the Student's *t* test (reported at 95% confidence level) and the degree to which the ensemble members agree on the sign of the anomalies. For the

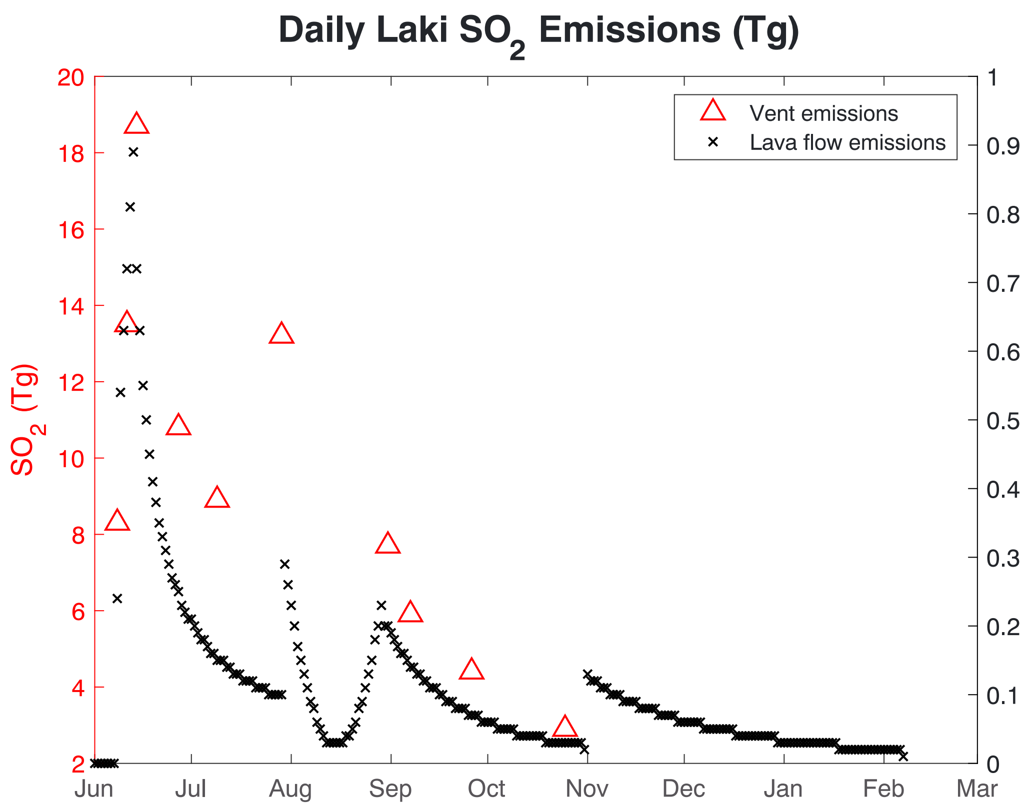

Figure 1. Daily mass of SO_2 gas emissions (Tg) for the Laki eruption 8 June 1783 to 7 February 1784, based on Figure 2 from Thordarson and Self (2003). The left *y* axis and red triangles correspond to the vent emissions, while the right *y* axis and black x marks correspond to lava flow emissions at the surface. Tick marks on the *x* axis represent the first day of the month indicated.

latter, we base the method on binomial probability: If the data were random (i.e., anomalies unforced), we would expect at least 27 of the ensemble members to agree on the sign of the anomaly 4% of the time. In this way, this method is similar to calculating a 95% confidence interval.

3. Results

3.1. Evolution of the Laki Aerosol Cloud

Figure 2 shows the zonal mean and NH mean sulfate aerosol optical depth (AOD at 550 nm) for the Laki ensemble from June 1783 to May 1784. The maximum optical depth perturbations in the ensemble mean occur near the pole and are above 1.3 in August (Figure 2a). The peak area-weighted NH average AOD of 0.45 also occurs in August (Figure 2b). As the model does not output AOD values where there is no solar radiation (Figure 2a; e.g., latitudes poleward of 70°N in boreal winter months), these times and latitudes are excluded from the NH average calculation plotted in Figure 2b; this results in a decrease (<15%) in the NH average AOD anomalies. The simulated *e*-folding lifetime of the Laki volcanic aerosols is 3–4 months, which is in good agreement with Oman, Robock, Stenchikov, Thordarson, Koch et al. (2006), Kravitz and Robock (2011), and Pausata, Grini, et al. (2015). This short lifetime is due to the low injection height of the SO_2 gas and the stratospheric circulation at high latitudes (Schmidt et al., 2016). As a result, most of the aerosols have been removed by May 1784, with the NH average AOD well below 0.1. The magnitude of the AOD perturbations is in better agreement with Oman, Robock, Stenchikov, Thordarson, Koch et al. (2006) than other, more recent modeling studies of Laki-style volcanic eruptions. Pausata, Grini, et al. (2015) found much larger maxima in the optical depth, with a NH average AOD anomaly above 1.4 in August. This is partially because the first eruption of their simulations was quite large, with a total emission of 34 Tg of SO_2 from 100 to 300 hPa, compared to the 8.3 Tg used in this study. However, the major source of differences in AOD and radiative forcing comes from differences in particle size, which are discussed below.

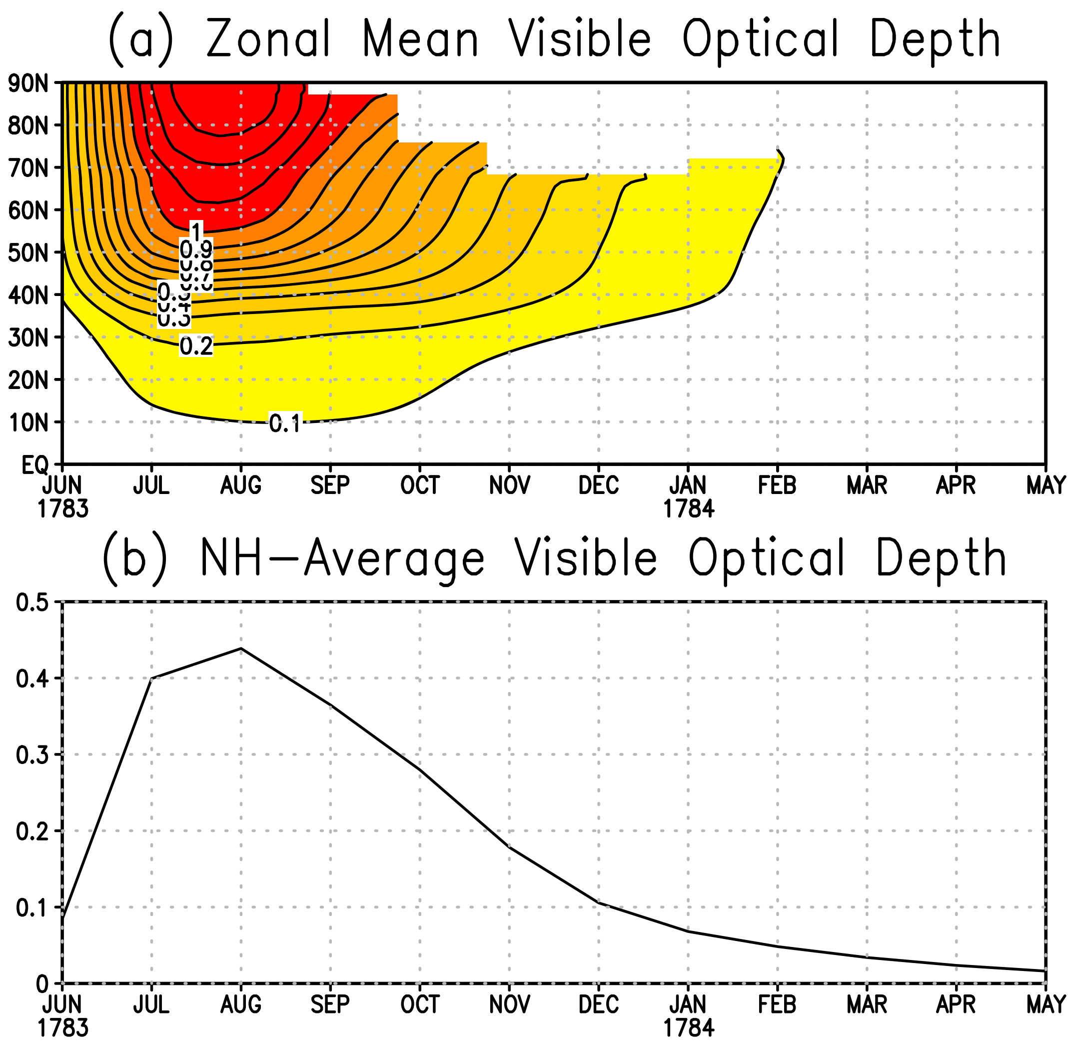

Figure 2. (a) Zonal mean and (b) Northern Hemisphere (NH) mean sulfate aerosol optical depth anomaly at 550 nm for the Laki ensemble from June 1783 to May 1784.

The amount of visible radiation reflected and scattered by volcanic aerosols depends strongly on the particle size distribution, with smaller particles scattering light more efficiently per unit mass. However, this key parameter remains, to some extent, poorly constrained. Pausata, Grini, et al. (2015) found an aerosol effective radius of about 0.2 μm in their simulations because the aerosols do not grow by self-coagulation in their model; this is 2–3 times smaller than the average effective radius in Oman, Robock, Stenchikov, Thordarson, Koch, et al. (2006; 0.54–0.61 μm). On the other hand, Oman, Robock, Stenchikov, Thordarson, Koch et al. (2006) based their effective radii on the study of Pinto et al. (1989), which evaluated modal sulfate aerosol radii produced by eruptions of different magnitudes using a one-dimensional model. Oman, Robock, Stenchikov, Thordarson, Koch et al. (2006) concluded that, based purely on the difference in cumulative SO_2 emissions between Pinatubo and Laki, their Laki aerosols should have effective radii about 20% larger than the 0.2–0.4 μm observed in the months after Pinatubo (Russell et al., 1996). However, while simulations by Pausata et al. (2016) might have had a lower estimate of the effective radii, Oman, Robock, Stenchikov, Thordarson, Koch et al. (2006) probably overestimated the effective radii, since the 94 Tg of SO_2 emitted in explosive episodes by Laki was not in a single day like Pinatubo but in 10 episodes over a 4-month span. In addition, as opposed to the high-altitude, tropical injection of Pinatubo, which yielded longer lifetimes, a lower effective radius is probably reasonable for the Laki eruption, which injected into the lower stratosphere at high latitude, yielding a shorter-lived aerosol cloud due to more wet removal and mixing.

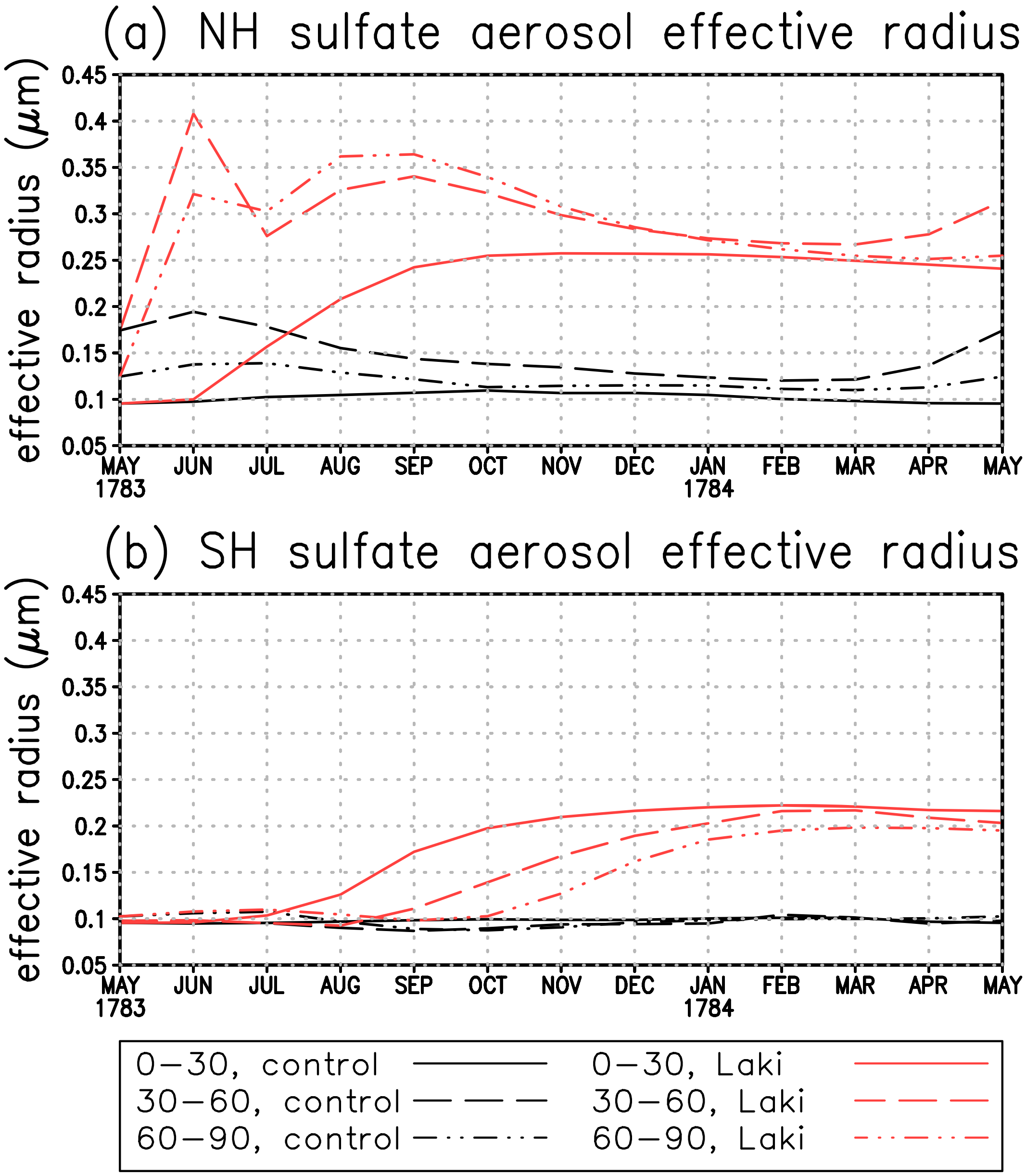

Figure 3. Zonal mean surface area density-weighted sulfate aerosol effective radius averaged over different latitude-height bins in the (a) Northern Hemisphere (NH) and (b) Southern Hemisphere (SH). For 0–30° bins, the 50- to 100-hPa range is used; for 30–60° and 60–90° bins, the 50- to 250-hPa range is used.

Figure 3 shows the grid-weighted average effective radii for different latitude-height bins for the control and Laki simulations using CESM1(WACCM). Here, the evolution of the Laki aerosol particle size is simulated by the three-section MAM3, which does not require any assumptions about the particle size. The effective radii are also weighted by the sulfate aerosol surface area density. The black lines show that, at all latitudes and for all seasons, the effective radius in the control simulation ranges from 0.1 to 0.2 μm. Particle growth occurs in regions with elevated sulfate concentrations at the beginning of the volcanic eruption (Figure 4). The maximum effective radius of 0.4 μm occurs at midlatitudes in June 1783, concurrent with the first and largest sulfur injections. In July, the average effective radius in the 30–60°N band decreases substantially, owing to a further increase in aerosol number there (not shown). Because of the location of the SO_2 gas injection from the Laki eruption (supporting information Figure S1), the largest increases in sulfate aerosol effective radius are simulated at NH middle and high latitudes. After the initial peak in June and subsequent reduction in July, the aerosol effective radii reach peak average values of approximately 0.34 and 0.36

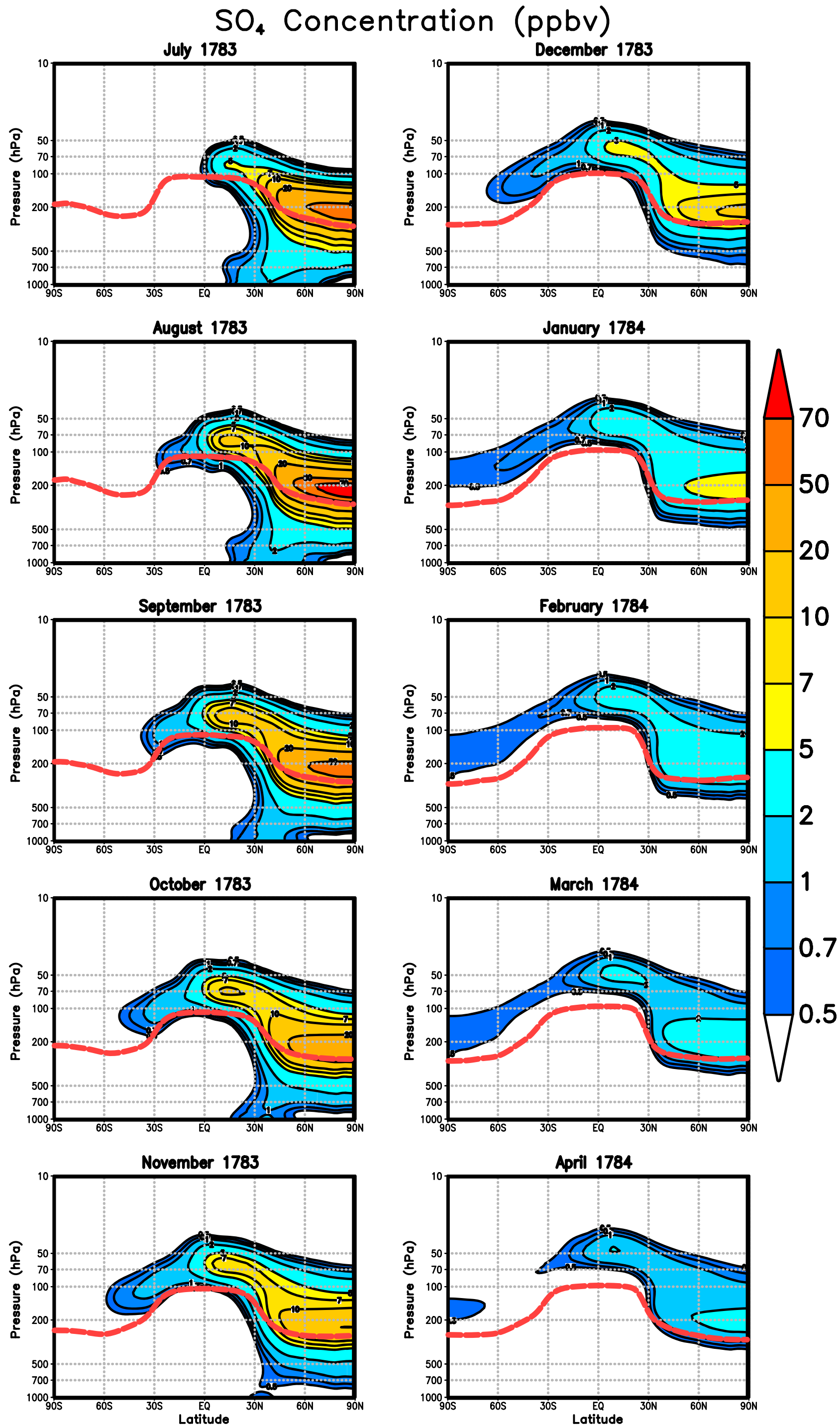

Figure 4. Zonal mean sulfate aerosol concentration (ppbv) for the Laki ensemble mean. The red line shows the model tropopause from the Laki simulations.

μm for the 30–60°N and 60–90°N latitude bins, respectively (Figure 3a). After July, the sulfate aerosol number density at NH midlatitudes (30–60°N) decreases linearly, as opposed to the number densities at polar and tropical NH latitudes, which decay exponentially with time. This implies that, although sulfuric acid vapor from the subsequent eruptive episodes can condensate onto existing particles, this growth competes with the formation of new aerosol particles, which can limit the increase in effective radius.

While the maxima at middle and high latitudes occur in September 1783, the peak average effective radius in the 0–30°N bin of approximately 0.25 μm is reached in October 1783, delayed by the equatorward transport of the aerosol. By December 1783 and thereafter, the average effective radius is about 0.25–0.3 μm for the entire NH. In the SH, the aerosol effective radii reach peak values near 0.2 μm, with slightly larger particles in the SH tropics (0–30°S; Figure 3b). Similarly to the delayed peak effective radius in the NH tropics, an extended delay is seen in the SH, with peak values occurring in January (0–30°S), February (30–60°S), and March 1784 (60–90°S). Overall, the effective radii simulated here lie in between the values in Pausata et al. (2016) and Oman, Robock, Stenchikov, Thordarson, Koch, et al. (2006). These results are in agreement with Schmidt et al. (2016), who found smaller aerosol burdens and sizes per unit SO_2 injection for flood lava eruptions compared to explosive eruptions, due to rapid removal and sustained depletion of OH in the upper troposphere/lower stratosphere region.

Figure 4 shows the temporal evolution of the sulfate aerosol concentrations in the Laki aerosol cloud. The maximum concentration of sulfate aerosols is in the lowermost stratosphere at high latitudes; this concentration increases from the initial injection in June until August, with a maximum concentration above 70 ppbv at 200 hPa and north of 60°N. After August, the concentrations at middle and high latitudes decrease and are everywhere below 2 ppbv by April 1784. Both sulfate aerosols and SO_2 gas (Figure 5) reach the NH tropical lower stratosphere, with a maximum aerosol concentration above 10 ppbv in September there. Figure 4 shows that once the aerosols reach the NH tropics—either by direct transport of the aerosols or by aerosol formation from SO_2 gas transported to the tropical stratosphere—they can be transported farther into the SH, with some aerosols even reaching the South Polar stratosphere (0.5–0.7 ppbv) by January 1784 (see supporting information Movie S1, also at http://people.envsci.rutgers.edu/bzambri/haze200.gif, for a movie of the global transport of SO_2 gas and sulfate aerosols from the Laki eruption simulations). This represents a significant perturbation to the stratospheric aerosol burden, as present-day background aerosol concentrations in the tropical stratosphere are typically below 0.5 ppbv (e.g., Brühl et al., 2015). With the Laki aerosol cloud making its way to the tropics and even crossing into the SH, significant though short-lived circulation impacts are detectable, as we show in section 3.2.

3.2. Impacts on Atmospheric Circulation

Following the Laki eruption, CESM1(WACCM) simulates significant zonal wind and temperature anomalies globally. Figure 6 shows the zonal mean zonal wind and temperature anomalies for each month starting with August 1783, where anomalies here are calculated by subtracting the mean of the 5 years before the eruption from the Laki ensemble mean. As expected, stratospheric heating coincides with the location of the sulfate aerosols. Specifically, the maximum heating in August is in the lower stratosphere, in the 50–70°N latitude bin. However, as the aerosols are transported equatorward, the location of the maximum stratospheric heating anomaly also shifts. By October 1783, the maximum anomaly, above 3 K, has shifted from 60°N and 200 hPa to 30°N and 70–100 hPa. A proposed mechanism for a forced weakening of stratospheric zonal winds is the opposite of the enhanced temperature gradient mechanism for tropical volcanic eruptions: Aerosols at high latitudes heat the polar stratosphere, weakening the temperature gradient and by thermal wind balance weakening the zonal winds. However, due to the transport of aerosols to the equatorial stratosphere, this region, too, is heated, and the temperature gradient therefore remains largely unaffected, at least through February 1784; this is further explored in section 3.3. In March 1784, though, after much of the aerosols have been removed from the equatorial stratosphere, large warming in the NH polar stratosphere is accompanied by a large weakening of the polar stratospheric westerlies at 60°N, with negative zonal wind anomalies extending to the surface. In contrast to the sparse response in the NH stratosphere, a robust and persistent tropospheric zonal wind response is seen there, with positive zonal wind anomalies south of 30°N, centered at 200 hPa. Starting in October and November, and reemerging in January 1784, the positive anomalies in the tropics are accompanied by negative zonal wind anomalies at midlatitudes, forming a dipole anomaly that suggests an equatorward shift of the NH subtropical jet stream that persists into April 1784. Pausata, Chafik, et al. (2015) and Pausata et al. (2016) found a positive anomaly in the El Niño–Southern Oscillation (ENSO) in response to a Laki-type eruption, and Zambri et al. (2019) found the same response in these simulations. In order to explore the relationship between the ENSO response and the equatorward shift of the subtropical jet, we performed a simple linear regression of the zonal wind anomalies onto the Niño 3.4 index. Figure 8a shows the relative fit based on the regression, and

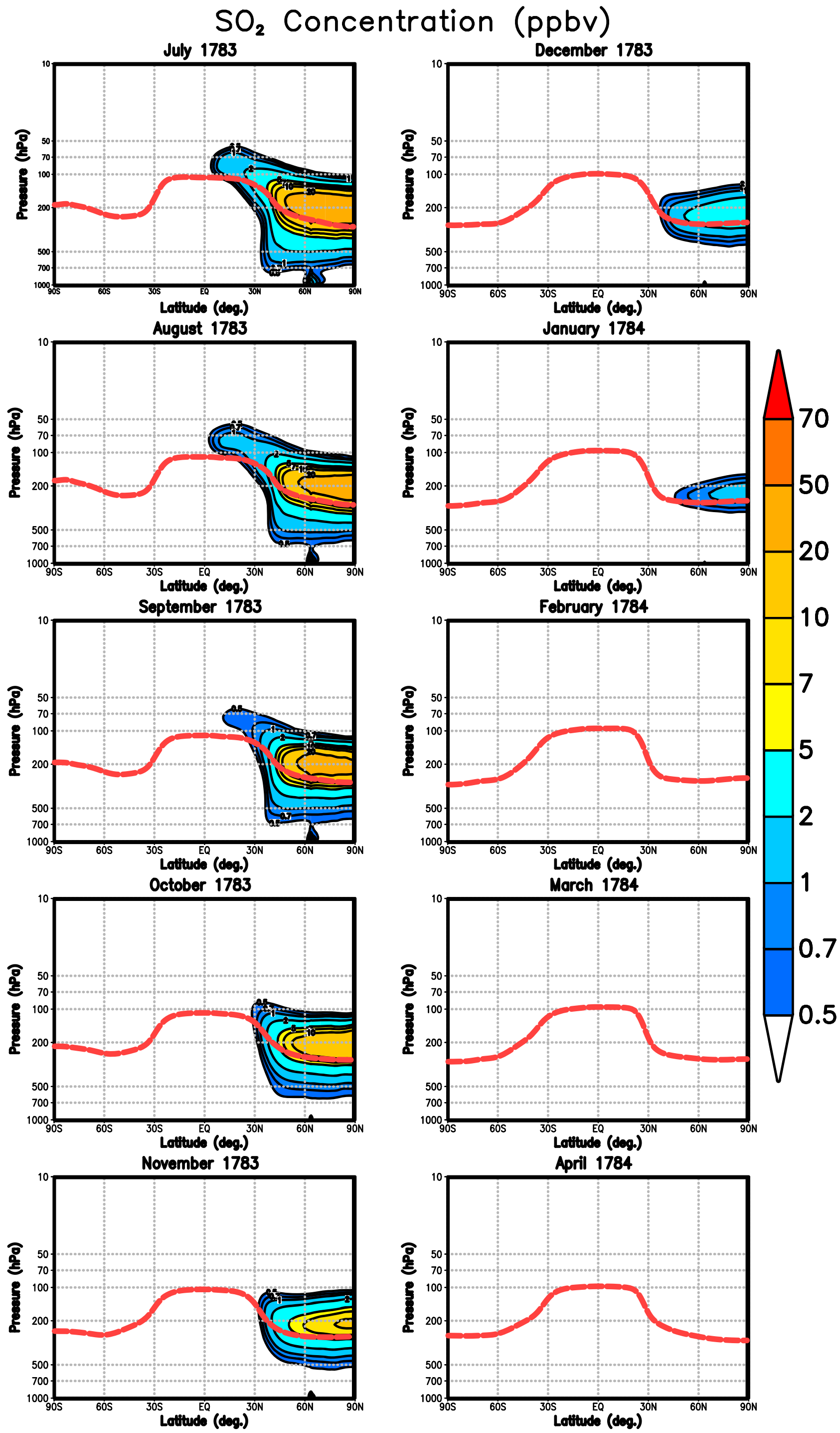

Figure 5. Zonal mean SO_2 concentration (ppbv) for the Laki ensemble mean. The red line shows the model tropopause from the Laki simulations.

Figure 8b shows the Niño 3.4 time series for the Laki ensemble mean. Figure 8c shows the residual zonal wind anomalies for Laki minus noLaki, after the ENSO influence has been removed, which show that much of the change in the tropospheric jet in Figures 6 and 7, prior to January 1784 in particular, can be attributed to the ENSO response. The persistence of the jet shift into January–March 1784 is related to the reduction of the midlatitude high pressure, which is also explored in Zambri et al. (2019).

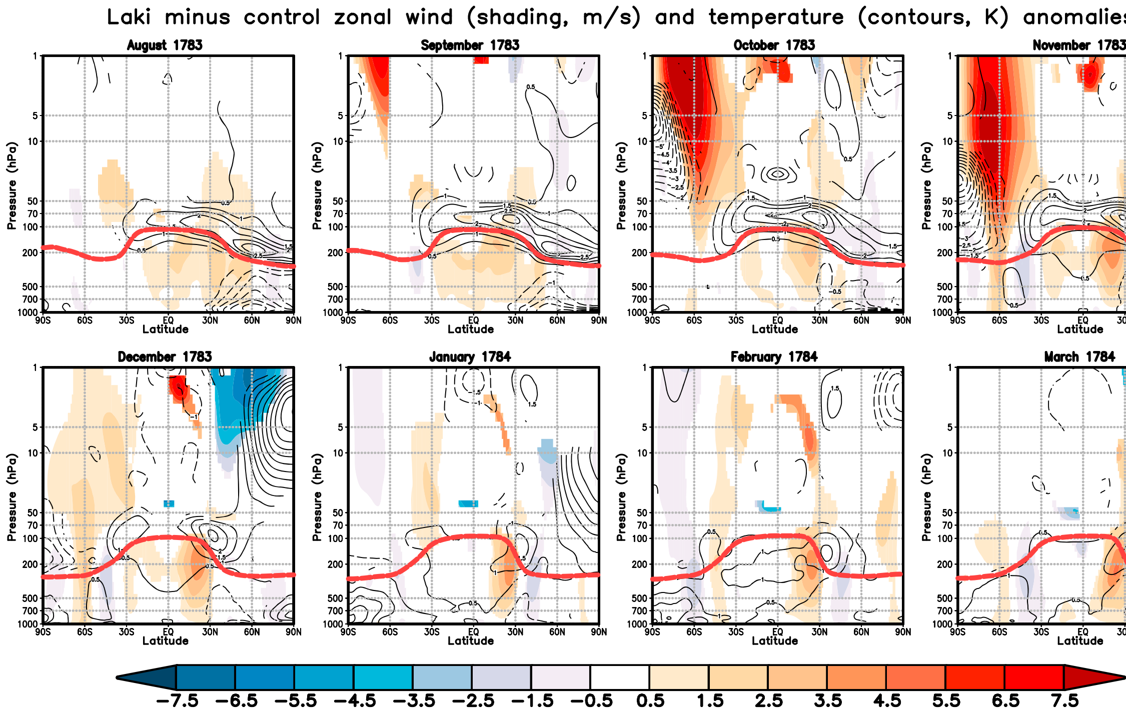

Figure 6. Zonal mean zonal wind (shading, m/s) and temperature (contours, K) anomalies for the Laki ensemble mean. Anomalies are calculated with respect to the 5 years before the eruption. Only anomalies significant at the 95% level using a Student's *t* test are plotted. The red line shows the model tropopause from the Laki simulations.

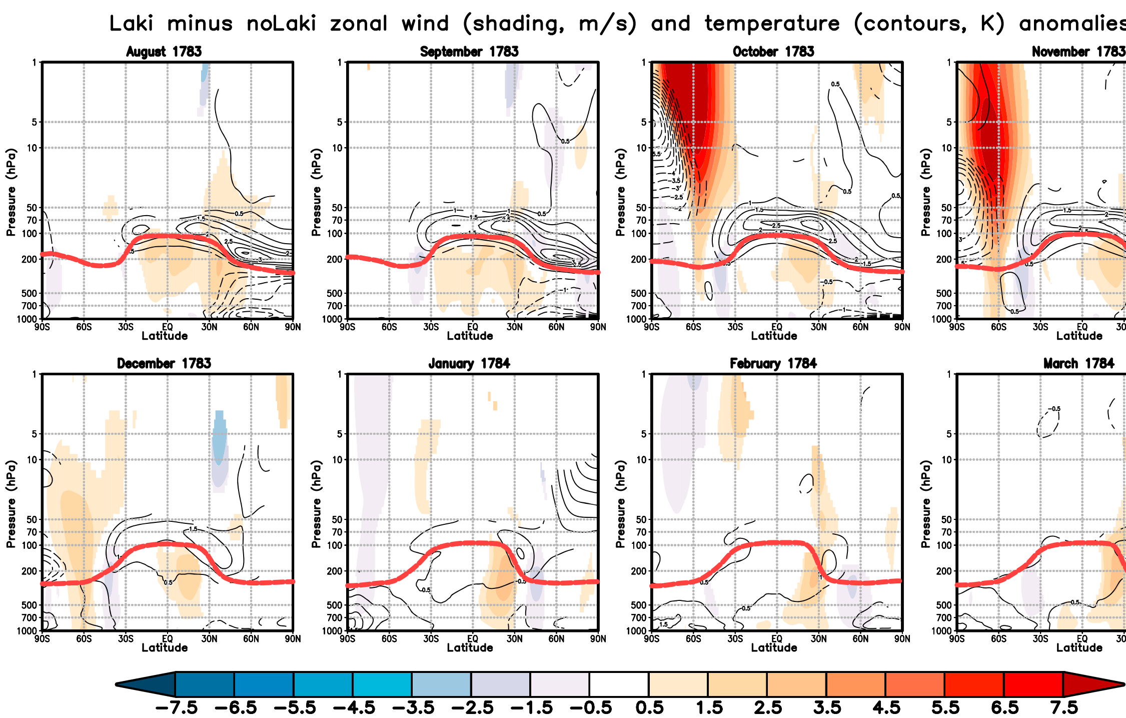

Figure 7. Same as Figure 5 but with anomalies calculated by subtracting the noLaki ensemble mean.

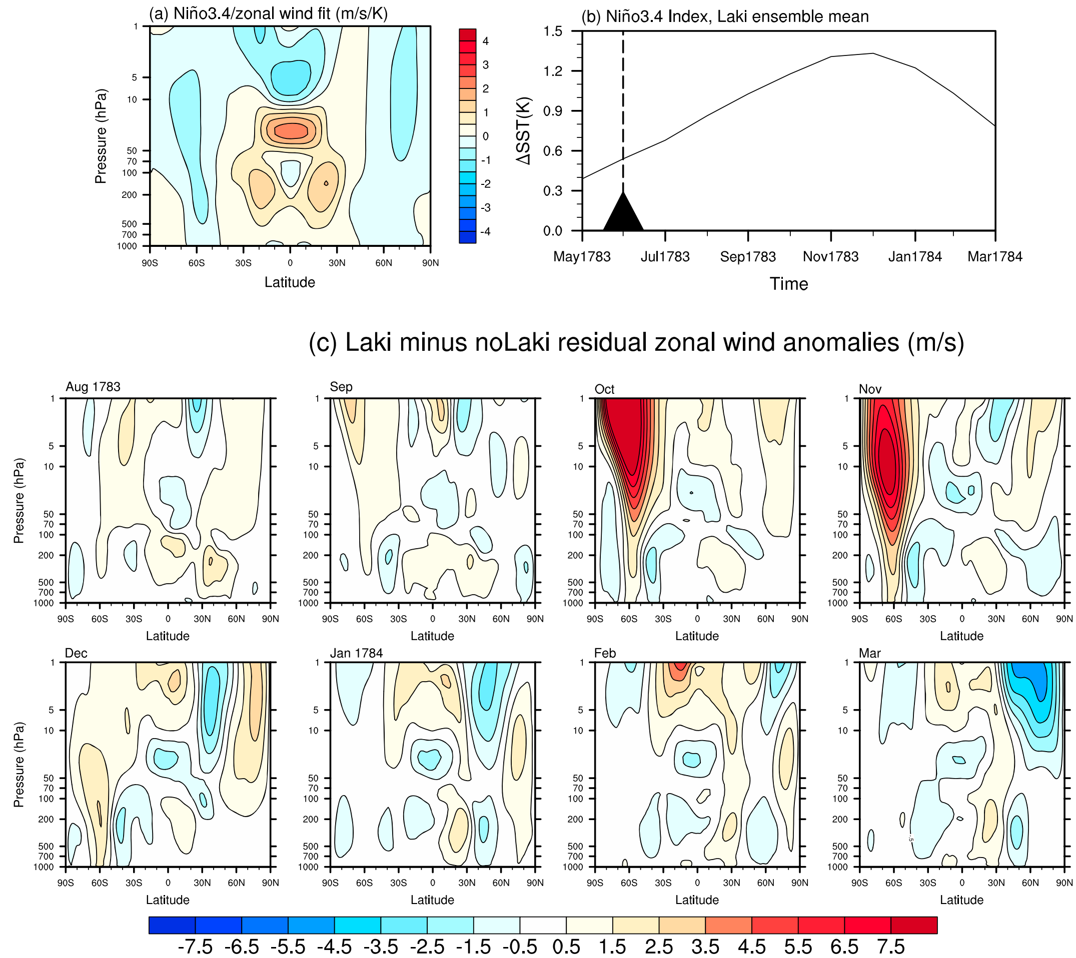

Figure 8. (a) Regression fit for Niño 3.4 index versus zonal wind (m/s/K), (b) Laki ensemble mean Niño 3.4 index (K), and (c) residual zonal mean zonal wind anomalies (m/s) after Niño 3.4 regression for Laki minus noLaki.

Perhaps somewhat surprisingly, the most robust circulation changes occur in the SH, with a response that is similar to the simulated stratospheric response to the 1991 Pinatubo eruption (e.g., Barnes et al., 2016). As the aerosols make their way to the equator and farther south, significant heating anomalies occur in the tropical stratosphere of both hemispheres. In August and September, this heating is accompanied by a slight increase in westerly winds starting near 30°S but shifting poleward with time. By October, the circulation changes likely result in a positive feedback: With the intensification of the polar vortex, less warm air is transported to the pole, further enhancing the temperature gradient. In October and November, strong westerly wind anomalies at 60°S extend from the stratosphere to the surface and are accompanied by large cooling at the pole, reaching 6 K in November. In these months, the westerly anomalies extend to 30°S in the stratosphere and all the way to the pole in November. The strengthened SH polar vortex continues into December 1783, though both the stratospheric heating anomalies and the magnitude of the zonal wind anomalies are considerably lower in magnitude at this point. By January 1784, the heating in the SH equatorial stratosphere has dissipated, and with it go the zonal wind anomalies.

In Figure 7, the zonal wind and temperature anomalies are calculated by subtracting the noLaki ensemble mean from the Laki ensemble mean. While many of the temperature anomalies are robust to the method of anomaly calculation, contrasting Figures 6 and 7 shows some substantial differences in the forced zonal wind response. Specifically, Figure 7 shows that the strengthened zonal winds at 60°S in September 1783 are unforced and related to the background initial conditions, as the anomaly vanishes when subtracting the noLaki ensemble mean from the Laki ensemble mean. In addition, much of the large warming and weakened zonal winds in the NH polar middle stratosphere in December 1783 vanish when using this method of anomaly calculation. Figure 7 also shows that several signals seen in Figure 6 are robust to the definition of the forced signal: the SH polar vortex strengthening in October–December, the large warming and weakened zonal winds in the NH polar stratosphere in March 1784, and the poleward shifted jet in the NH midlatitude troposphere, though this pattern is in general weaker in Figure 7 than Figure 6.

The circulation response to low-latitude volcanic eruptions can be evaluated by examining the Southern Annular Mode (SAM) or NAM/NAO response (e.g., Barnes et al., 2016). We performed the same analysis for this high-latitude volcanic eruption, and the results for the SAM and NAM are plotted in Figure 9. We define the SAM and NAM, at each pressure level, as the leading empirical orthogonal function of the monthly mean zonally averaged anomalous zonal winds between 20° and 80° latitude of the respective hemispheres, as in Barnes et al. (2016). The leading principal components (the annular mode time series) are standardized by subtracting the mean value of the 25-year control run and dividing by the standard deviation. In Figures 8a and 8b, the spatial patterns of the SAM and NAM, respectively, are shown. A positive tropospheric annular mode index is traditionally defined such that the jet stream is strengthened and shifted poleward relative to climatology; a positive value in the stratosphere denotes strengthened zonal winds relative to climatology (e.g.Baldwin & Dunkerton, 1999, Barnes et al., 2016). Figures 8c and 8d show the Laki ensemble mean SAM and NAM time series, respectively. Figure 9c displays a significant positive SAM anomaly in both the stratosphere and troposphere in the months following the eruption. There is also a positive SAM anomaly in June, immediately following the eruption, but this anomaly is likely not related to the eruption, due to the time needed for the transport of the volcanic aerosols (e.g., Figure 4). However, from August until December 1783, there is a significant strengthening of the SAM, with as many as 37 of 40 ensemble members agreeing on the sign of the anomaly. In the troposphere, a weaker positive SAM anomaly is also simulated from September until December 1783. In this case, up to 34 of the 40 ensemble members agree on the sign of the anomaly, with the most agreement near the surface in November 1783. Based on the high level of ensemble agreement, this appears to be a robust SAM response to a NH high-latitude eruption.

Much like the zonal wind anomalies in Figures 6 and 7, the simulated NAM and SAM responses are quite different. In the NH stratosphere, only a small negative NAM response is simulated in December 1783 and shows little agreement between ensemble members. On the other hand, there is a longer-lasting negative NAM signal in the troposphere and lowermost stratosphere. The negative anomaly begins in July 1783 in the 100- to 200-hPa range and from there strengthens and extends downward into the troposphere, reaching its maximum extent and intensity in late winter (January to March 1784), and remaining until April 1784. This anomaly also exhibits generally high agreement. Both the magnitude and the level of ensemble agreement of this anomaly are greatest at 200 hPa; this is consistent with the dipole anomaly in Figures 6 and 7, which was the largest signal in the NH there. We calculated the SAM and NAM time series for the noLaki ensemble as well, and Figures 9e and 9f show the difference between the Laki and noLaki ensemble mean time series. Figure 9e shows, similarly to Figure 7, that the SH anomalies prior to October are more related to initial/background conditions than the volcanic eruption itself, but that the October–December anomalies are a robust Laki response. Figure 9f shows similar NAM patterns to Figure 9d, but with the anomalies generally a bit weaker and the negative NAM in December 1783 vanishing; this, too, is in agreement with the differences between Figures 6 and 7 in the NH.

3.3. Temperature Gradient Response

We begin here by demonstrating the relationship between the equator-to-pole temperature gradient and the polar vortex strength in each hemisphere. We compute the quantity U_{10}, defined as the anomaly in the zonal mean, zonal wind at 10 hPa and 60°S/N. This quantity is frequently used as an indicator of polar vortex strength (e.g.Butler & Gerber, 2018, Charlton & Polvani, 2007, Toohey et al., 2014). We also compute ∇T_{50}, the lower stratospheric temperature gradient defined as the difference in zonal mean temperature between the tropics (30°S–30°N) and the pole (60–90°N/S) at 50 hPa in each hemisphere. The relationship between anomalies in U_{10} and ∇T_{50} is shown in Figure 10. In the SH, the relationship is strongest in austral spring, with Pearson correlation coefficients of 0.87, 0.96, and 0.98 in September, October, and November, respectively. In the NH, a strong relationship is evident from October through April, with Pearson correlation coefficients above 0.9 in all months except October, for which the correlation is 0.86.

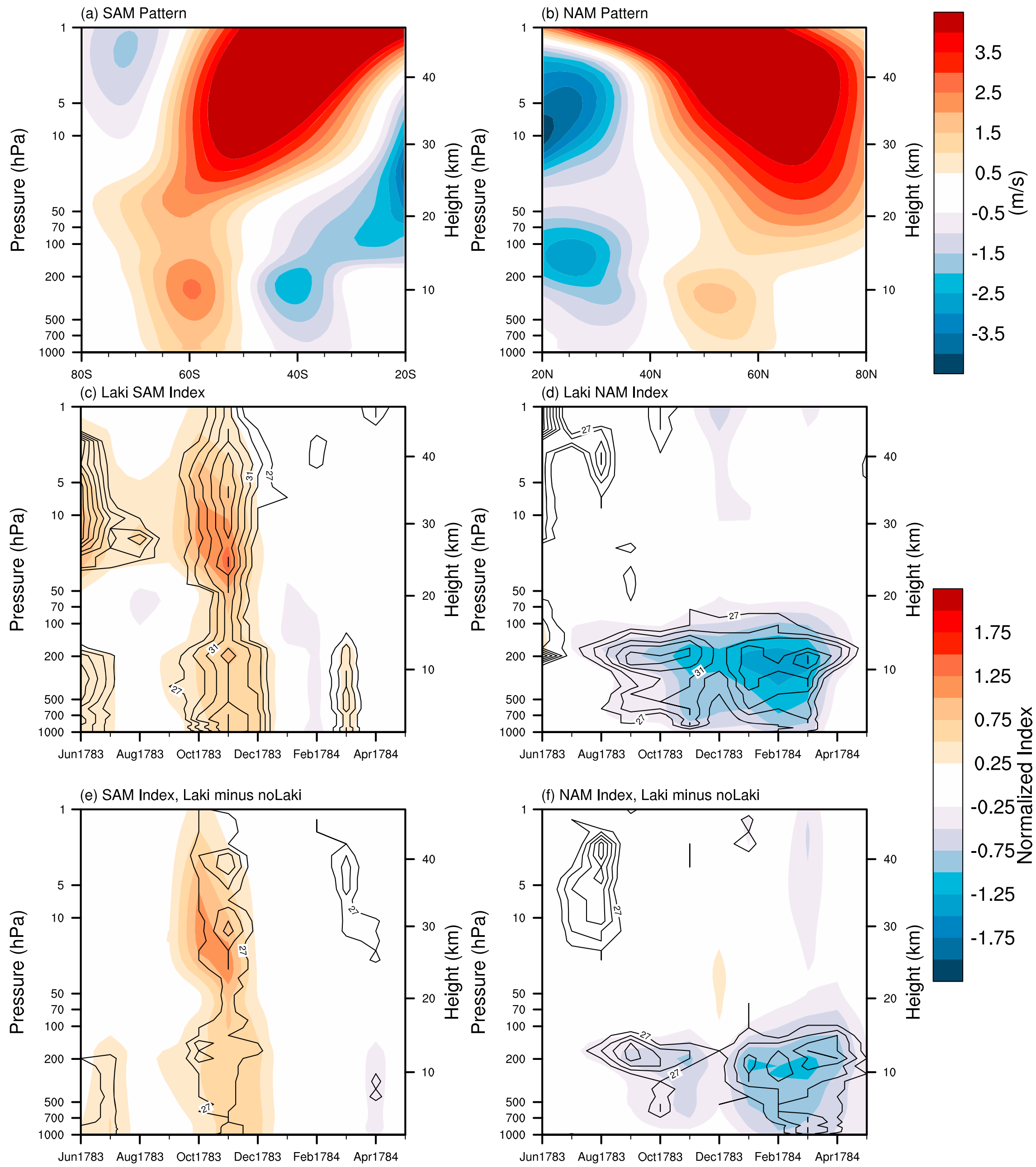

Figure 9. Spatial patterns of the (a) Southern Annular Mode (SAM) and (b) Northern Annular Mode (NAM) (m/s), and normalized time series of the SAM and NAM for the Laki ensemble mean (c and d) and for the difference between the Laki and noLaki ensemble means (e and f). Contours in (c)–(f) represent the number of ensemble members (out of 40) that agree on the sign of the anomaly, with only contours ≥27 shown to represent statistical significance at the 95% level.

Figures 10 and 11 show the 50-hPa zonal mean temperature anomalies and temperature gradient anomalies. In the SH tropics, there is a 1–2 K warming at 50 hPa beginning in August until December 1783, along with cooling up to 6 K near the pole that lasts until November. However, these anomalies are calculated with respect to the 5 years before the Laki eruption. By computing the same anomalies for the noLaki ensemble (i.e., noLaki minus control), it is clear that the large cooling at the SH pole in August and September, which could otherwise be interpreted as a volcanic response, is identical in both ensembles: The anomaly has more to do with the background state than the volcanic perturbation. Without belaboring this point, we turn now to those anomalies that are uniquely associated with the Laki ensemble. The positive temperature anomalies

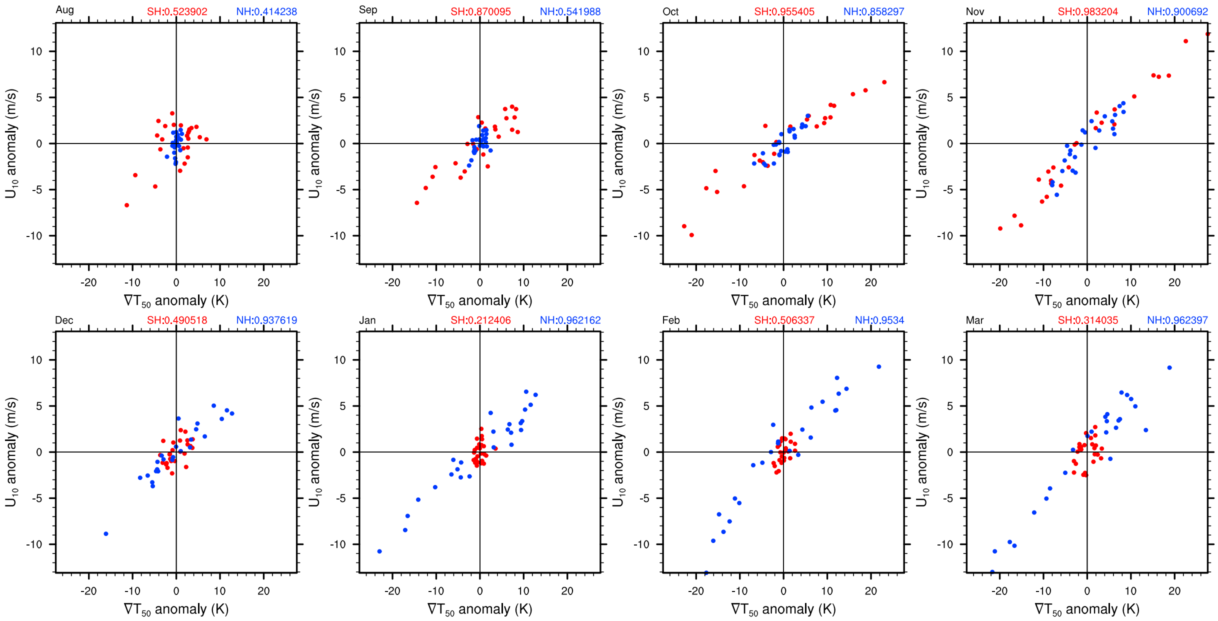

Figure 10. Scatter plots of the 50-hPa temperature gradient anomaly between 60–90° and −30–30° versus the 10-hPa zonal wind anomaly at 60° for the Southern Hemisphere (SH; red) and Northern Hemisphere (NH; blue) for the 25-year control run. Numbers at top middle and top right of each panel are the Pearson correlation coefficients for the SH and NH, respectively. SH = Southern Hemisphere; NH = Northern Hemisphere.

in the SH are clearly a response to the Laki eruption, with the largest anomalies (both with respect to the control run and the noLaki ensemble) occurring in October and November. The negative anomalies poleward of 50°S in August–November appear in both ensembles, though the polar stratosphere is 2–4 K colder for the Laki ensemble than the noLaki ensemble in October and November. Figure 12 further illustrates this point, with nearly identical temperature gradient perturbations in August and September, but with the Laki ensemble showing strengthened temperature gradients from ~20°S and poleward in

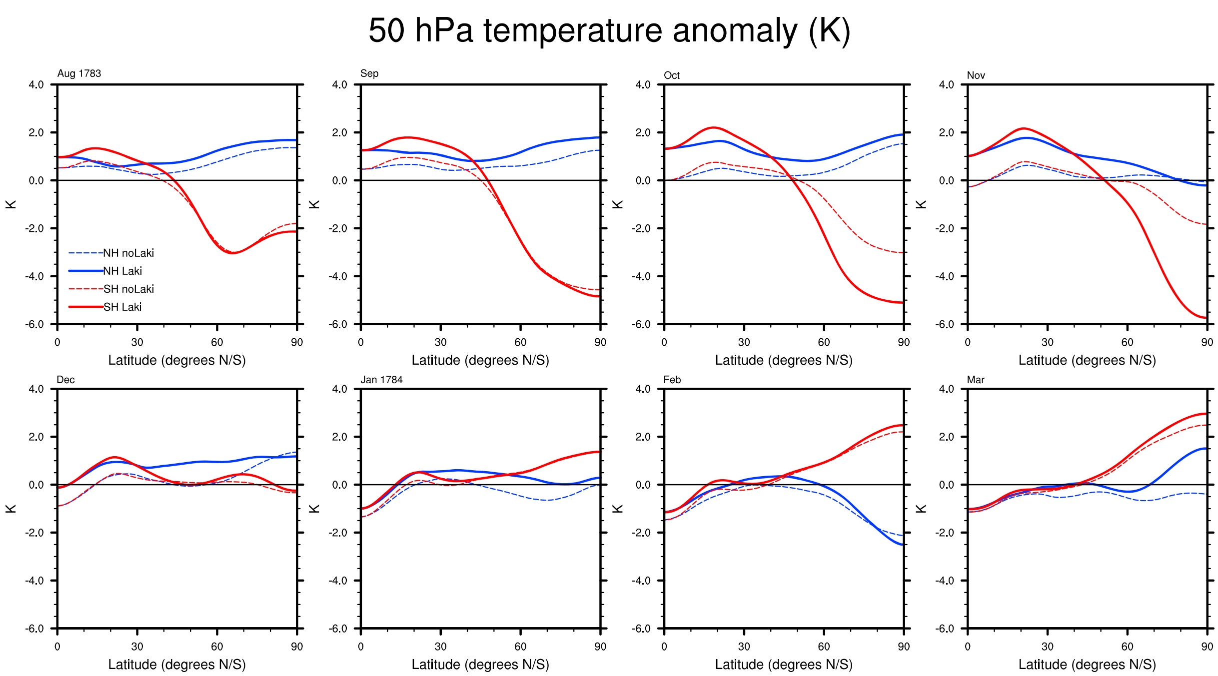

Figure 11. The 50-hPa temperature anomaly (K) for Northern Hemisphere (NH; blue) and Southern Hemisphere (SH; red) for the Laki (solid lines) and noLaki (dashed lines) ensembles. Anomalies calculated with respect to the 5 years before the Laki eruption.

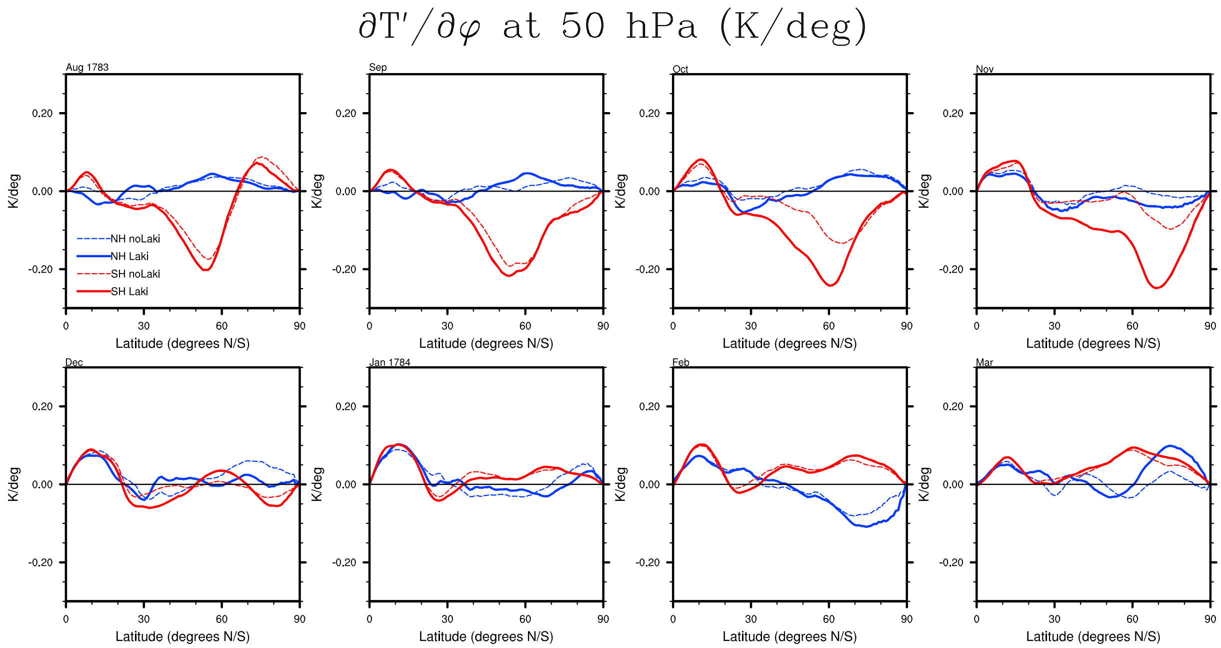

Figure 12. The 50-hPa temperature gradient anomaly (K/deg) for Northern Hemisphere (NH; blue) and Southern Hemisphere (SH; red) for the Laki (solid lines) and noLaki (dashed lines) ensembles. Anomalies calculated with respect to the 5 years before the Laki eruption.

October and November, relative to the noLaki ensemble and to the control run. The maximum temperature gradient perturbation of 0.25 K/deg occurs precisely at 60°S in October and near 70°S in November. Figures 10 and 11 show that, while the strong polar vortex in August and September was unforced, its continued strength and persistence into October and November was forced by the Laki eruption and specifically the warming of the tropical lower stratosphere.

In the NH lower stratosphere, the maximum heating of ~2 K occurs near 20°N in October and November 1783 (Figure 11). There is heating at middle and high latitudes as well, with anomalies of ~1 K between 30°N and 60°N, and anomalies between 1 and 2 K poleward of 60°N in August–October, though these anomalies do not appear to be significant when viewed in comparison to the similar anomalies in the noLaki ensemble. As a result of the similar heating across latitudes, Figure 12 shows that the temperature gradients in the NH remain largely unperturbed, with anomalies everywhere within ±0.1 K/deg.

3.4. Wave-Driven Circulation Response

In addition to the lower stratospheric meridional temperature gradient, the polar vortex strength is controlled by planetary wave drag and therefore depends on the upward wave flux from the troposphere into the stratosphere (Newman et al., 2001; Polvani & Waugh, 2004). We have computed the transformed Eulerian mean diagnostics (Andrews et al., 1987) in order to assess changes in wave driving forced by the Laki eruption. Laki ensemble anomalies of the vertical component of the Eliassen-Palm flux (F_z) and the Eliassen-Palm flux divergence (EPFD) are plotted in Figure 13, and anomalies in the meridional residual mass circulation stream function, ψ^*, are plotted in Figure 14. F_z is indicative of the amount of wave activity entering the stratosphere, while EPFD determines the amount of wave drag, with positive values causing reduced wave drag and an acceleration of the westerly zonal winds and decreasing the poleward residual circulation. The climatological meridional residual circulation is poleward in both hemispheres. Therefore, positive anomalies in Figure 14 (red contours) indicate a *reduced* poleward residual circulation in the SH and an *increased* poleward residual circulation in the NH. Anomalies shown in Figures 13 and 14 are calculated as the difference between the Laki ensemble and the 5 years before the eruption.

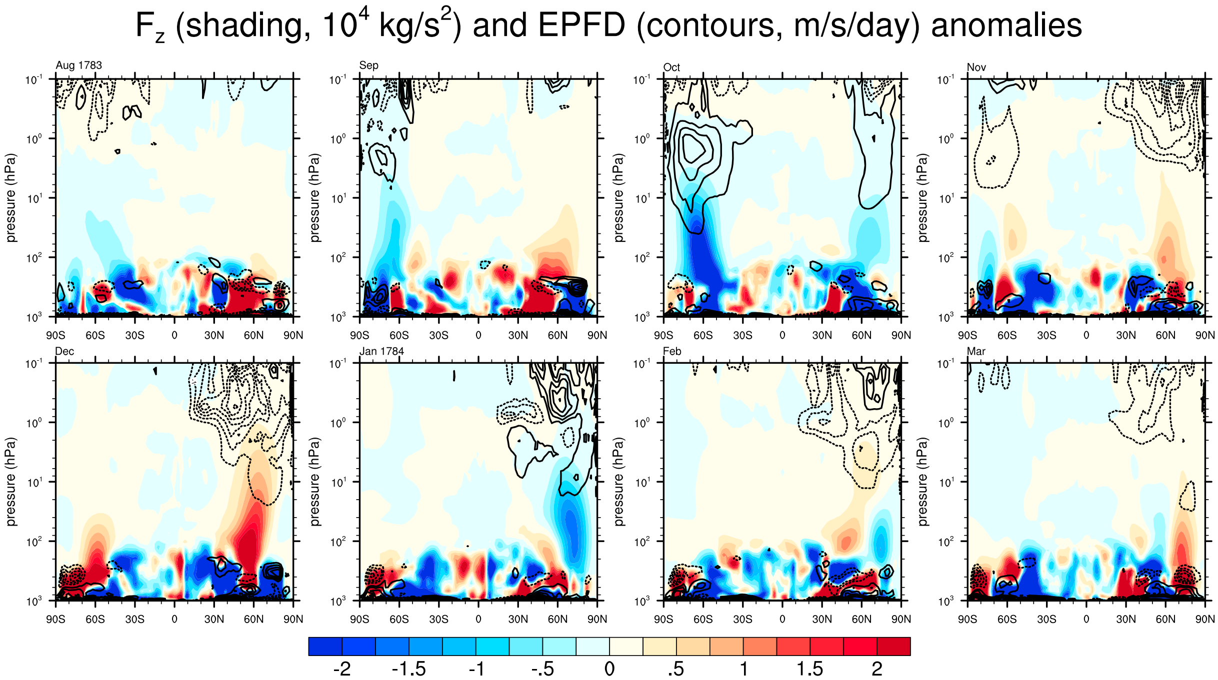

Figure 13. Anomalies of the vertical component of Eliassen-Palm (EP) flux (F_z, 10^4 kg/s^2, shading) and the EP flux divergence (EPFD, m/s/day, contours) for the Laki ensemble mean. EPFD contours are in units of 0.5 m/s/day.

In the SH, the largest wave forcing is in October 1783, when the Laki ensemble shows large negative F_z anomalies from 40°S and poleward, beginning at about 200 hPa and upward, which indicates fewer waves entering the SH stratosphere. This is further illustrated by the positive EPFD anomalies, which are indicative of less wave drag. As a result, the poleward residual circulation is reduced throughout the SH stratosphere in October (Figure 14). On the other hand, while the 50-hPa temperature gradient remains perturbed in

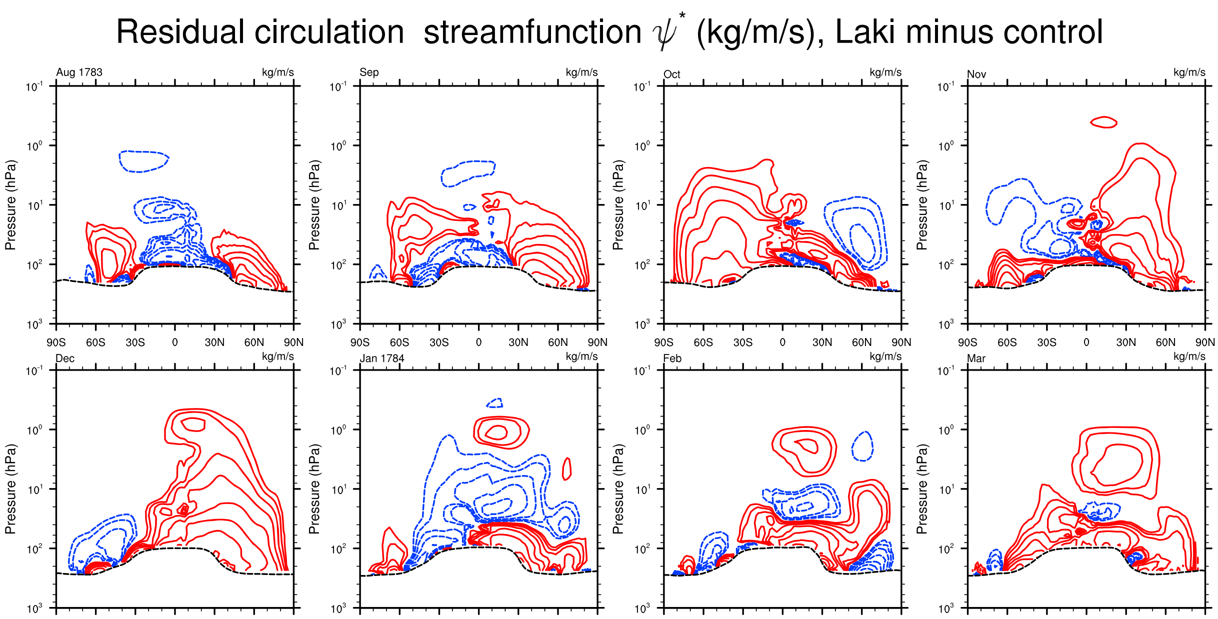

Figure 14. Residual circulation streamfunction (kg/m/s), Laki ensemble mean minus control. Positive contours are red, and negative contours are blue. Contour intervals are log spaced from ±1 to ±100 kg/m/s (approximately ±1, 1.7, 2.8, 4.6, 7.7, 12.9, 21.5, 35.9, 59.9, and 100). The black line shows the model tropopause from the Laki simulations.

November (Figure 12), the wave forcing in November and December acts to decelerate the vortex, showing enhanced wave drag (negative EPFD anomalies) and increased F_z in the stratosphere poleward of 30°S (Figure 13), along with a slightly increased poleward residual circulation (Figure 14). Yet, in spite of the wave forcing acting to decelerate the SH vortex, significant strengthening persists in November 1783 (Figures 6–9). This shows that perturbations to the meridional temperature gradient, along with the wave forcing, are important for the SH polar vortex response to a NH high-latitude eruption.

In the NH, the Laki eruption generally tends to increase wave activity and the poleward residual circulation, with positive F_z anomalies north of 30°N and from 100–200 hPa and upward, and negative EPFD anomalies (Figure 13) inducing a poleward residual circulation (Figure 14). This NH wave forcing does appear to drive significant warming of the NH polar middle stratosphere in December and March 1784. The largest EPFD anomalies tend to be above 5 hPa. Two exceptions are October 1783 and January 1784, during which months the opposite response is seen, with negative F_z and positive EPFD anomalies leading to an equatorward residual circulation anomaly in the lowermost NH midlatitude stratosphere above 100 hPa. The oscillatory nature of the NH wave forcing in the Laki ensemble can help to explain why more significant and persistent temperature and zonal wind responses are not seen in the lower stratosphere. Laki minus noLaki anomalies are not shown for the transformed Eulerian mean diagnostics, but the differences based on the anomaly calculation methods are consistent with the previous results: The most robust changes in stratospheric wave driving attributed to the volcanic eruption are in the SH in October and November.

4. Summary and Discussion

We simulated the evolution of the stratospheric aerosol cloud from the 1783–1784 Laki eruption in Iceland and its associated circulation impacts using CESM1(WACCM), which is able to explicitly simulate the evolution of stratospheric sulfate aerosols. We found significant transport of SO_2 gas and sulfate aerosols in both hemispheres, as well as robust circulation changes on a global scale. Due to the high latitude and relatively low altitude of injection, the lifetime of the Laki aerosols is relatively short. As a result, and because of the timing of the eruption (i.e., the seasonality), the anomalies did not fall into typical seasonal categories and were better identified on a monthly basis (e.g., the strongest SH responses were found in October, November, and December). We identified robust responses using the statistical significance of the anomalies, as well as degree to which the ensemble agreed on the sign of the response. The main results from the CESM1(WACCM) Laki simulations are summarized as follows:

1. The Laki aerosols as simulated by CESM1(WACCM) have a peak effective radius ranging from about 0.2 to 0.4 μm, with an average effective radius near 0.3 μm in the NH lower stratosphere.
2. SO_2 gas injected into the upper troposphere/lower stratosphere at high latitudes and the subsequent SO_4 aerosols are transported to the SH at significant mixing ratios (up to 5 ppbv SO_4 in the SH tropics and ~0.5 ppbv SO_4 at the South Pole).
3. Robust wind and temperature responses are simulated in both hemispheres in the months after the onset of the NH high-latitude eruption.
4. The SAM response extends from the stratosphere to the troposphere, lasting about 3 months and peaking about 5 months after the beginning of the eruption, in SH spring.
5. The NAM response is longer lasting but more confined to the troposphere; this response is strongest in the boreal late winter/spring and is related to the ENSO forcing as well as pressure changes at the surface (Zambri et al., 2019).
6. The choice of base period for computing anomalies, that is, subtracting the mean of some control period or the mean of an equivalent ensemble without the volcanic perturbation, can significantly alter the perceived "forced response" to a volcanic eruption, in agreement with the analysis in Pausata, Grini, et al. (2015).

Stevenson et al. (2003) mentioned the transport of a small amount of SO_4 into the SH. Oman, Robock, Stenchikov, Thordarson, Koch et al. (2006), found that the aerosol cloud was confined mostly to latitudes north of 30°N but did mention some transport south of 30°N. Schmidt et al. (2010), using a global aerosol model, simulated the transport of significant amounts of SO_4 south of the equator, though they simulated maximum concentrations of only about 1 ppbv SO_4 in the SH and analyzed resulting changes in SH cloud condensation nuclei. Trigo et al. (2009) reported possible observations of the Laki haze as far south as Brazil, though these observations occurred in September and October 1784, by which time most of the aerosols would have fallen out of both hemispheres in the simulations presented here. While this study is in agreement with past studies in that the bulk of the aerosol remains confined in the NH, we have shown that the transport of aerosol into the SH (>2 ppbv maximum in this study) is more important than previously thought.

Related to the far-reaching transport of the Laki aerosols, we found significant circulation responses in the SH stratosphere and troposphere in the form of a strengthening of the polar vortex. This response is qualitatively similar to the expected response to a large tropical volcanic eruption (e.g. Barnes et al., 2016, Karpechko et al., 2010). Specifically, we find, like Karpechko et al. (2010) found for simulations of the low-latitude El Chichón and Pinatubo eruptions, that the SH polar vortex is strengthened, with zonal wind anomalies above 8 m/s in austral spring, when planetary waves have the most impact on the stratospheric circulation there. In October 1783 we find that, indeed, a reduction in wave breaking in the polar stratosphere and reduced poleward residual circulation help drive the polar vortex strengthening. It is also likely, in view of the lack of a circulation response found in JJA by Robock et al. (2007), that this Laki response is dependent on the timing of the eruption; in other words, a high-latitude eruption in March, resulting in the arrival of the aerosol in the tropics and their subsequent heating of the lower stratosphere in June–August, would have a much more minimal effect on the SH circulation.

On the other hand, the circulation response in the NH is quite different. Because heating by volcanic aerosols occurs at both high and low latitudes, the temperature gradients in the NH stratosphere are not perturbed to any great extent, and the NH stratospheric circulation remains largely unchanged. Instead, the largest zonal wind changes occur near 30°N and 200 hPa, where circulation changes in the troposphere (e.g., ENSO and NAO) cause an equatorward shift of the subtropical jet that lasts from August 1783 until March 1784. This response is somewhat different from what was observed after the twentieth century low-latitude El Chichón and Mount Pinatubo eruptions (e.g., Stenchikov et al., 2006). Specifically, Stenchikov et al. (2006) found that the Pacific jet moved equatorward (similar to this study) but that the Atlantic jet moved poleward (opposite results herein). The differences are related to different NAO responses, namely, a positive NAO response for low-latitude eruptions and a negative NAO response for their high-latitude counterparts; this contrast highlights an important difference in the response to low- and high-latitude eruptions.

It is customary to compute the forced volcanic response by subtracting the mean of an arbitrary period (here 5 years) before the volcanic perturbation from the period of interest following the perturbation. However, while this is conceptually done in order to remove the effect of the background state and internal variability, the volcanically perturbed period has its own internal variability, which can confound the forced response. We find that most of the anomalies deemed significant with respect to the mean of the 5 years before the eruption are also significant with respect to the unperturbed (noLaki) ensemble, though there are some exceptions. The results presented here support the conclusions of Pausata, Grini, et al. (2015), in that the latter method of calculating the anomaly (Laki minus noLaki) does a better job of separating the volcanically forced response from the background state and internal variability. Though we chose initial conditions based on the synoptic meteorology reported over western Europe around the time of the Laki eruption, the initial states of the large-scale climate features (e.g., ENSO, quasi-biennial oscillation, and NAO) vary between ensemble members. Therefore, though the initial conditions do not comprise every possible climate state, we do not believe this conclusion is dependent upon a particular choice of initial conditions.

The global impacts of high-latitude volcanic eruptions are far less studied than their low-latitude counterparts, in part because of the shorter lifetime of their emissions and therefore their impacts. However, the results in this study show that high-latitude volcanic eruptions can have significant impacts on global circulation on seasonal to annual timescales. These results advance our understanding of the impact of high-latitude volcanic eruptions and can therefore help to forecast the impacts of such an eruption in the future. Zambri et al. (2019) address the surface climate responses from the simulations discussed here. Because of the subannual scale of the responses presented here, the timing of the eruption will likely also play a role in the magnitude and duration of the responses (Kravitz and Robock, 2011). For example, Schmidt et al. (2010) showed how the seasonality of the onset of the eruption (e.g., starting on 8 December, rather than

8 June) can affect the chemical and microphysical effects of a Laki eruption; this would also affect the circulation and surface climate response, and simulation and analysis of such situations remains relevant for improving the ability to forecast climate after future volcanic eruptions.

Acknowledgments
This work is supported by National Science Foundation (NSF) grant AGS-1430051. The National Center for Atmospheric Research (NCAR) is supported by NSF. Simulations were conducted on the NCAR Yellowstone computer. The authors thank three anonymous reviewers for their thoughtful comments, which greatly improved the manuscript. Model output is available upon registration with the Harvard Dataverse (https://doi.org/10.7910/DVN/G1H3AC).

References

Andrews, D. G., Holton, J. R., & Leovy, C. B. (1987). *Middle atmosphere dynamics*. New York, USA: Academic Press.

Baldwin, M. P., & Dunkerton, T. J. (1999). Propagation of the Arctic Oscillation from the stratosphere to the troposphere. *Journal of Geophysical Research*, *104*(D24), 30,937–30,946. https://doi.org/10.1029/1999JD900445

Barnes, E., Solomon, S., & Polvani, L. (2016). Robust wind and precipitation responses to the Mount Pinatubo eruption, as simulated in the CMIP5 models. *Journal of Climate*, *29*(13), 4763–4778. https://doi.org/10.1175/JCLI-D-15-0658.1

Bittner, M., Schmidt, H., Timmreck, C., & Sienz, F. (2016). Using a large ensemble of simulations to assess the Northern Hemisphere stratospheric dynamical response to tropical volcanic eruptions and its uncertainty. *Geophysical Research Letters*, *43*, 9324–9332. https://doi.org/10.1002/2016GL070587

Bittner, M., Timmreck, C., Schmidt, H., Toohey, M., & Krüger, K. (2016). The impact of wave-mean flow interaction on the Northern Hemisphere polar vortex after tropical volcanic eruptions. *Journal of Geophysical Research: Atmospheres*, *121*, 5281–5297. https://doi.org/10.1002/2015JD024603

Brühl, C., Lelieveld, J., Tost, H., Höpfner, M., & Glatthor, N. (2015). Stratospheric sulfur and its implications for radiative forcing simulated by the chemistry climate model EMAC. *Journal of Geophysical Research: Atmospheres*, *120*, 2103–2118. https://doi.org/10.1002/2014JD022430

Butler, A. H., & Gerber, E. P. (2018). Optimizing the definition of a sudden stratospheric warming. *Journal of Climate*, *31*(6), 2337–2344. https://doi.org/10.1175/JCLI-D-17-0648.1

Charlton, A. J., & Polvani, L. M. (2007). A new look at stratospheric sudden warmings. Part I: Climatology and modeling benchmarks. *Journal of Climate*, *20*(3), 449–469. https://doi.org/10.1175/JCLI3996.1

Christiansen, B. (2008). Volcanic eruptions, large-scale modes in the Northern Hemisphere, and the El Niño–Southern Oscillation. *Journal of Climate*, *21*(5), 910–922. https://doi.org/10.1175/2007JCLI1657.1

Gettelman, A., Liu, X., Ghan, S. J., Morrison, H., Park, S., Conley, A. J., et al. (2010). Global simulations of ice nucleation and ice supersaturation with an improved cloud scheme in the Community Atmosphere Model. *Journal of Geophysical Research*, *115*, D18216. https://doi.org/10.1029/2009JD013797

Highwood, E. J., & Stevenson, D. S. (2003). Atmospheric impact of the 1783–1784 Laki eruption: Part II Climatic effect of sulphate aerosol. *Atmospheric Chemistry and Physics*, *3*(4), 1177–1189. https://doi.org/10.5194/acp-3-1177-2003

Hurrell, J. W. (1995). Decadal trends in the North Atlantic Oscillation: Regional temperatures and precipitation. *Science*, *269*(5224), 676–679. https://doi.org/10.1126/science.269.5224.676

Hurrell, J. W., Holland, M. M., Gent, P. R., Ghan, S., Kay, J. E., Kushner, P. J., et al. (2013). The Community Earth System Model: A framework for collaborative research. *Bulletin of the American Meteorological Society*, *94*(9), 1339–1360. https://doi.org/10.1175/BAMS-D-12-00121.1

Karpechko, A. Y., Gillett, N. P., Dall'Amico, M., & Gray, L. J. (2010). Southern Hemisphere atmospheric circulation response to the El Chichón and Pinatubo eruptions in coupled climate models. *Quarterly Journal of the Royal Meteorological Society*, *136*(652), 1813–1822. https://doi.org/10.1002/qj.683

Kington, J. A. (1988). *The weather of the 1780's over Europe*, 164 pp. New York: Cambridge University Press.

Koch, D., Schmidt, G., & Field, C. (2006). Sulfur, sea salt and radionuclide aerosols in GISS ModelE. *Journal of Geophysical Research*, *111*, D06206. https://doi.org/10.1029/2004JD005550

Kravitz, B., & Robock, A. (2011). Climate effects of high-latitude volcanic eruptions: Role of the time of year. *Journal of Geophysical Research*, *116*, D01105. https://doi.org/10.1029/2010JD014448

Liu, X., Easter, R. C., Ghan, S. J., Zaveri, R., Rasch, P., Shi, X., et al. (2012). Toward a minimal representation of aerosols in climate models: Description and evaluation in the Community Atmosphere Model CAM5. *Geoscientific Model Development*, *5*(3), 709–739. https://doi.org/10.5194/gmd-5-709-2012

Marsh, D., Mills, M., Kinnison, D. E., & Lamarque, J.-F. (2013). Climate change from 1850 to 2005 simulated in CESM1(WACCM). *Journal of Climate*, *26*(19), 7372–7391. https://doi.org/10.1175/JCLI-D-12-00558.1

Mills, M. J., Richter, J. H., Tilmes, S., Kravitz, B., MacMartin, D. G., Glanville, A. A., et al. (2017). Radiative and chemical response to interactive stratospheric sulfate aerosols in fully coupled CESM1(WACCM). *Journal of Geophysical Research: Atmospheres*, *122*, 13,061–13,078. https://doi.org/10.1002/2017JD027006

Mills, M. J., Schmidt, A., Easter, R., Solomon, S., Kinnison, D. E., Ghan, S. J., et al. (2016). Global volcanic aerosol properties derived from emissions, 1990–2014, using CESM1(WACCM). *Journal of Geophysical Research: Atmospheres*, *121*, 2332–2348. https://doi.org/10.1002/2015JD024290

Morrison, H., & Gettelman, A. (2008). A new two-moment bulk stratiform cloud microphysics scheme in the Community Atmosphere Model, Version 3 (CAM3). Part I: Description and numerical tests. *Journal of Climate*, *21*(15), 3642–3659. https://doi.org/10.1175/2008JCLI2105.1

Newman, P. A., Nash, E. R., & Rosenfield, J. E. (2001). What controls the temperature of the Arctic stratosphere during the spring? *Journal of Geophysical Research*, *106*(D17), 19,999–20,010. https://doi.org/10.1029/2000JD000061

Oman, L., Robock, A., Stenchikov, G., Schmidt, G. A., & Ruedy, R. (2005). Climatic response to high-latitude volcanic eruptions. *Journal of Geophysical Research*, *110*, D13103. https://doi.org/10.1029/2004JD005487

Oman, L., Robock, A., Stenchikov, G. L., Thordarson, T., Koch, D., Shindell, D. T., & Gao, C. (2006). Modeling the distribution of the volcanic aerosol cloud from the 1783–1784 Laki eruption. *Journal of Geophysical Research*, *111*, D12209. https://doi.org/10.1029/2005JD006899

Oman, L., Robock, A., Stenchikov, G. L., & Thordarson, T. (2006). High-latitude eruptions cast shadow over the African monsoon and the flow of the Nile. *Geophysical Research Letters*, *33*, L18711. https://doi.org/10.1029/2006GL027665

Pausata, F. S. R., Chafik, L., Caballero, R., & Battisti, D. S. (2015). Impacts of a high-latitude volcanic eruption on ENSO and AMOC. *Proceedings of the National Academy of Sciences of the United States of America*, *112*(45), 13,784–13,788. https://doi.org/10.1073/pnas.1509153112

Pausata, F. S. R., Grini, A., Caballero, R., Hannachi, A., & Seland, Ø. (2015). High-latitude volcanic eruptions in the Norwegian Earth System Model: The effect of different initial conditions and of the ensemble size. *Tellus B: Chemical and Physical Meteorology*, *67*(1), 26728. https://doi.org/10.3402/tellusb.v67.26728

Pausata, F. S. R., Karamperidou, C., Caballero, R., & Battisti, D. S. (2016). ENSO response to high-latitude volcanic eruptions in the Northern Hemisphere: The role of the initial conditions. *Geophysical Research Letters*, *43*, 8694–8702. https://doi.org/10.1002/2016GL069575

Pinto, J. P., Turco, R. P., & Toon, O. B. (1989). Self-limiting physical and chemical effects in volcanic eruption clouds. *Journal of Geophysical Research*, *94*(D8), 11,165–11,174. https://doi.org/10.1029/JD094iD08p11165

Polvani, L. M., & Waugh, D. W. (2004). Upward wave activity flux as a precursor to extreme stratospheric events and subsequent anomalous surface weather regimes. *Journal of Climate*, *17*(18), 3548–3554. https://doi.org/10.1175/1520-0442(2004)017<3548:UWAFAA>2.0.CO;2

Robock, A., Adams, T., Moore, M., Oman, L., & Stenchikov, G. (2007). Southern Hemisphere atmospheric circulation effects of the 1991 Mount Pinatubo eruption. *Geophysical Research Letters*, *34*, L23710. https://doi.org/10.1029/2007GL031403

Russell, P. B., Livingston, J. M., Pueschel, R. F., Bauman, J. J., Pollack, J. B., Brooks, S. L., et al. (1996). Global to microscale evolution of the Pinatubo volcanic aerosol derived from diverse measurements and analyses. *Geophysical Research Letters*, *101*(D13), 18,745–18,763. https://doi.org/10.1029/96JD01162

Schmidt, A., Carslaw, K. S., Mann, G. W., Wilson, M., Breider, T. J., Pickering, S. J., & Thordarson, T. (2010). The impact of the 1783–1784 AD Laki eruption on global aerosol formation processes and cloud condensation nuclei. *Atmospheric Chemistry and Physics*, *10*(13), 6025–6041. https://doi.org/10.5194/acp-10-6025-2010

Schmidt, A., Mills, M. J., Ghan, S., Gregory, J. M., Allan, R. P., Andrews, T., et al. (2018). Volcanic radiative forcing from 1979 to 2015. *Journal of Geophysical Research: Atmospheres*, *123*, 12,491–12,508. https://doi.org/10.1029/2018JD028776

Schmidt, A., Skeffington, R. A., Thordarson, T., Self, S., Forster, P. M., Rap, A., et al. (2016). Selective environmental stress from sulphur emitted by continental flood basalt eruptions. *Nature Geoscience*, *9*(1), 77–82. https://doi.org/10.1038/NGEO2588

Schmidt, A., Thordarson, T., Oman, L. D., Robock, A., & Self, S. (2012). Climatic impact of the long-lasting 1783 Laki eruption: Inapplicability of mass-independent sulfur isotopic composition measurements. *Journal of Geophysical Research*, *117*, D23116. https://doi.org/10.1029/2012JD018414

Stenchikov, G., Hamilton, K., Robock, A., Ramaswamy, V., & Schwarzkopf, M. D. (2004). Arctic Oscillation response to the 1991 Pinatubo eruption in the SKYHI GCM with a realistic Quasi-Biennial Oscillation. *Journal of Geophysical Research*, *109*, D03112. https://doi.org/10.1029/2003JD003699

Stenchikov, G., Hamilton, K., Stouffer, R. J., Robock, A., Ramaswamy, V., Santer, B., & Graf, H.-F. (2006). Arctic Oscillation response to volcanic eruptions in the IPCC AR4 climate models. *Journal of Geophysical Research*, *111*, D07107. https://doi.org/10.1029/2005JD006286

Stenchikov, G., Robock, A., Ramaswamy, V., Schwarzkopf, M. D., Hamilton, K., & Ramachandran, S. (2002). Arctic Oscillation response to the 1991 Mount Pinatubo eruption: Effects of volcanic aerosols and ozone depletion. *Journal of Geophysical Research*, *107*(D24), 4803. https://doi.org/10.1029/2002JD002090

Stevenson, D. S., Johnson, C. E., Highwood, E. J., Gauci, V., Collins, W. J., & Derwent, R. G. (2003). Atmospheric impact of the 1783–1784 Laki eruption: Part I Chemistry modelling. *Atmospheric Chemistry and Physics*, *3*(3), 487–507. https://doi.org/10.5194/acp-3-487-2003

Thompson, D. W. J., & Wallace, J. M. (1998). The Arctic Oscillation signature in the wintertime geopotential height and temperature fields. *Geophysical Research Letters*, *25*(9), 1297–1300. https://doi.org/10.1029/98GL00950

Thordarson, T. (1995). *Volatile release and atmospheric effects of basaltic fissure eruptions*, Ph.D. thesis. Honolulu: University of Hawaii.

Thordarson, T., & Self, S. (2003). Atmospheric and environmental effects of the 1783–1784 Laki eruption: A review and reassessment. *Journal of Geophysical Research*, *108*(D1), 4011. https://doi.org/10.1029/2001JD002042

Thordarson, T., Self, S., Oskarsson, N., & Hulsebosch, T. (1996). Sulfur, chlorine, and fluorine degassing and atmospheric loading by the 1783–1784 AD Laki (Skaftár Fires) eruption in Iceland. *Bulletin of Volcanology*, *58*(2-3), 205–225. https://doi.org/10.1007/s004450050136

Toohey, M., Krüger, K., Bittner, M., Timmreck, C., & Schmidt, H. (2014). The impact of volcanic aerosol on the Northern Hemisphere stratospheric polar vortex: Mechanisms and sensitivity to forcing structure. *Atmospheric Chemistry and Physics*, *14*(23), 13,063–13,079. https://doi.org/10.5194/acp-14-13063-2014

Toohey, M., Krüger, K., Sigl, M., Stordal, F., & Svensen, H. (2016). Climatic and societal impacts of a volcanic double event at the dawn of the Middle Ages. *Climate Change*, *136*(3-4), 401–412. https://doi.org/10.1007/s10584-016-1648-7

Trigo, R., Vaquero, J., & Stothers, R. B. (2009). Witnessing the impact of the 1783–1784 Laki eruption in the Southern Hemisphere. *Climate Change*, *99*, 535–546.

Vehkamäki, H., Kulmala, M., Napari, I., Lehtinen, K., Timmreck, C., Noppel, M., & Laaksonen, A. (2002). An improved parameterization for sulfuric acid-water nucleation rates for tropospheric and stratospheric conditions. *Journal of Geophysical Research*, *107*(D22), 4622. https://doi.org/10.1029/2002JD002184

Zambri, B., LeGrande, A. N., Robock, A., & Slawinska, J. (2017). Northern Hemisphere winter warming and summer monsoon reduction after volcanic eruptions over the last millennium. *Journal of Geophysical Research: Atmospheres*, *122*, 7971–7989. https://doi.org/10.1002/2017JD026728

Zambri, B., & Robock, A. (2016). Winter warming and summer monsoon reduction after volcanic eruptions in Coupled Model Intercomparison Project 5 (CMIP5) simulations. *Geophysical Research Letters*, *43*, 10,920–10,928. https://doi.org/10.1002/2016GL070460

Zambri, B., Robock, A., Mills, M. J., & Schmidt, A. (2019). Modeling the 1783–1784 Laki eruption in Iceland, part II: Climate impacts. *Journal of Geophysical Research: Atmospheres*. https://doi.org/10.1029/2018JD029554